

國 立 清 華 大 學

博 士 論 文

前瞻金屬氧化物與低溫多晶矽薄膜電晶體

開發與物理機制探討

Development and Physical Mechanisms Establishment of
Advanced Metal Oxides and Low-Temperature Polysilicon
Thin-Film Transistors

系別：電子工程研究所

學號：106063529

研 究 生：涂玉發(Yu-Fa Tu)

指 導 教 授：連振忻(Chen-Hsin Lien)

張鼎張(Ting-Chang Chang)

中 華 民 國 一 一 三 年 一 月

摘要

近年來，隨著人工智慧與電動車的快速發展，帶動相關科技產業蓬勃發展。其中，顯示器已廣泛應用於各類產品中，也促進相關產業的研究發展。在顯示器中，薄膜電晶體是最為關鍵的零組件，其特性與可靠度的品質好壞，將會決定面板的顯示效果，因此薄膜電晶體的電性需要進一步提升，以應用於新興的科技產品中。本論文研究銦鎵鋅氧與低溫多晶矽薄膜電晶體的電性與可靠度，釐清其相關的物理機制，並提出物理模型，用以推動顯示器產業的發展。

在金屬氧化物薄膜電晶體方面，其具有寬能隙、低漏電、透明、均勻性好等優點，適合應用於各類顯示器產品。其中，銦鎵鋅氧材料具有穩定的沉積品質，因此最為廣泛當作薄膜電晶體的通道層，然而其性能與可靠度仍需進一步改善。在第三章中，提出一具有源端延伸金屬電極結構的銦鎵鋅氧薄膜電晶體，可提升元件的通道控制能力，抑制漏致勢壘降低效應，其具有穩定的飽和輸出電流特性，可以改善面板的導線壓降所造成發光不均勻的問題，進而提升整體像素的亮度均勻性，且也可以改善熱載子效應。此外，在第四章中，源端延伸金屬電極結構可保護銦鎵鋅氧的源端不受到外界紫外光照射影響，可改善負偏壓照光不穩定性的問題，提升薄膜電晶體的可靠度。在第五章中，銦鎵鋅氧材料易受水氣影響，導致電性劣化，因此提出一保護層的材料組合，可改善水氣對元件的影響，且正偏壓不穩定性與熱載子效應的可靠度亦能維持相同特性。

在低溫多晶矽薄膜電晶體方面，其具有高載子遷移率與高穩定性，適合用於高階與可撓式顯示器產品。隨著未來微發光二極體顯示器的技術發展，P 型低溫多晶矽薄膜電晶體的電流已不足以應用於下一世代的顯示產品，因此急需開發 N 型低溫多晶矽薄膜電晶體。在第六章中，探討不同汲與源極接觸孔洞密度對 N 型低溫多晶矽薄膜電晶體的特性與自熱效應相關的不穩定性影響，當元件的接觸孔洞密度越大，可降低汲與源極的接觸電阻，且不增加額外的寄生電容，改善電阻-電容延遲特性。然而，在大電流操作下，接觸孔洞密度越大的元件會發生嚴重的扭結效應與自熱效應，導致電性劣化，因此對於特定產品的應用，汲與源極接觸孔洞密度是需要詳細考量的因素之一。

此外，柔性面板的應用產品越來越廣泛，因此薄膜電晶體在機械應力下的特性與可靠度需詳細釐清，以確保面板的優良運作。在第七章中，探討元件在不同機械應力條件下對汲極偏壓不穩定性的影響。在通道長度方向的壓應力下，強大的應力集中在元件的閘/源極與閘/汲極處，導致閘極絕緣層產生缺陷，因此當施加汲極偏壓時，電子會大量注入到缺陷中，導致電性嚴重裂化，因此對於可撓式驅動電晶體的應用，元件在通道寬度方向的壓應力下，會有較好的汲極偏壓不穩定性可靠度。

關鍵字:薄膜電晶體、銦鎳鋅氧、低溫多晶矽、熱載子效應、負偏壓照光不穩定性、正偏壓不穩定性、水氣、自熱效應、可撓、機械應力



Abstract

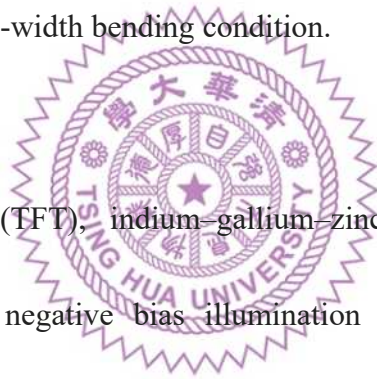
In recent years, the rapid development of artificial intelligence and electric vehicles has driven significant growth in related technology industries. In particular, displays have found widespread applications in various products, further promoting development and research in related fields. Among displays, thin-film transistors (TFTs) are the most critical component, with their performances and reliabilities significantly impacting panel display quality. As a result, it is essential to enhance the electrical properties of TFTs to meet the demands of emerging technology products. This dissertation investigates the electrical performances and reliabilities of Indium-Gallium-Zinc Oxide (IGZO) and low-temperature polycrystalline silicon (LTPS) based TFTs, elucidating their underlying physical mechanisms and presenting physical models. These efforts aim to drive advancements in the display industry.

In the realm of metal oxide TFTs, they possess several advantages such as wide bandgap, low leakage current, transparency, and excellent deposition uniformity, making them well-suited for various display products. Among these, IGZO stands out for its consistently high-quality deposition, making it the most widely employed channel material in TFTs. However, there is still room for further enhancement in its performances and reliabilities. In Chapter 3, a source-extended metal electrode structure design for IGZO TFTs is proposed. This structure can enhance the device's channel control capability to reduce drain-induced barrier lowering effect. It exhibits stable saturated output current characteristics, which can mitigate the IR-drop phenomenon, subsequently enhancing overall pixel

brightness uniformity in panels. In addition, it can also enhance the hot-carrier stability. Furthermore, in Chapter 4, the source-extended metal electrode structure serves to shield the source region of a-IGZO from UV light exposure. Consequently, this improvement effectively addresses the issue of negative bias illumination stress instability, subsequently enhancing the reliability of TFTs. In Chapter 5, it is noted that IGZO material is susceptible to moisture, leading to electrical degradation. Therefore, a combination of passivation (PV) layer materials is proposed to mitigate the impact of humidity on TFTs. As a result, the optimized combination of PV materials can mitigate the impact of the moist environment during positive bias stress and improve the hot-carrier stability.

In the realm of LTPS TFTs, they exhibit high carrier mobility and stability, making them suitable for advanced and flexible display products. However, with the ongoing technological developments in micro light-emitting diode displays, the current value of P-type LTPS TFTs is no longer sufficient for next-generation display applications. Therefore, there is an urgent necessity to develop N-type LTPS TFTs. In Chapter 6, the effect of the n-type LTPS TFTs with variant source/drain contact hole densities on performance and self-heating-related instability is analyzed. Devices with a greater number of contact holes demonstrate decreased contact resistance without introducing extra parasitic capacitance, thereby improving the RC delay characteristic. However, under high current operation, devices with higher contact hole density experience a severe kink effect and self-heating effect, resulting in electrical degradation. Therefore, the divergence in beneficial characteristics provides flexibility, and the choice between the devices with variant contact hole densities will depend on the specific demands of displays technology.

Furthermore, as the application of flexible displays becomes increasingly widespread, it's crucial to thoroughly understand the performances and reliabilities of TFTs under mechanical bending stress to ensure the reliable operation of display. In Chapter 7, the effect of different uniaxial mechanical bending conditions on drain bias stress (DBS) in flexible LTPS TFTs is analyzed. Under the compressive-length bending condition, a significant stress concentration at the GI near the gate/drain and gate/source regions induces the generation of numerous defects in these regions. Consequently, under DBS, a substantial injection of electrons into these defects occurs, resulting in severe electrical degradation. Therefore, for driving TFTs in flexible displays, it's found that devices exhibit better DBS reliability under compressive-width bending condition.



Keywords: thin-film transistor (TFT), indium-gallium-zinc oxide (IGZO), low-temperature polysilicon (LTPS), hot-carrier, negative bias illumination stress, positive bias stress, moist environment, self-heating stress, flexible, mechanical bending.

致謝

時光匆匆，在這篇論文完成之際，我誠摯地感謝所有在我學術生涯中給予我無盡支持、鼓勵和幫助的人。你們的支持和鼓勵對我來說是無價之寶，使我能夠克服各種困難，取得這項重要的學術成就。

首先，我要衷心感謝我的指導教授，清華大學的連振圻老師與中山大學的張鼎張老師，感謝你們的悉心指導和知識分享，你們的專業指導和博學多才讓我能夠不斷成長，最終實現了這一重要成就。此外，我萬分感謝張鼎張老師提供了完善且優良的實驗室環境，讓我在博士班期間能無後顧之憂的研究，使我翻轉人生，最終完成博士學位，並進入一流公司就業。

我也特別感謝校內口試委員林崇榮教授、金雅琴教授、吳孟奇教授、張鑑元教授，以及校外口試委員台積電莊文獻處長、台積電褚立新經理、國立清華大學徐碩鴻教授撥冗審查我的論文，並在口試時給予我寶貴的指導，使我的博士論文更加完善，特此感謝。

在博士班期間，我要感謝資深的學長學姊們，包括莫亦先、陳紀文、傅棕晟、陳敏甄、朱哲丘、陳柏勳，你們的經驗分享和建議對我的研究提供了寶貴的指引。此外，我也要特別感謝廖柏詠學長、蘇婉菁學姊、陳宏誌學長與洪揚豪學長對我的指導，不論是初入實驗室時的基本知識的建立，或是在後期的研究討論，甚至是對於人處事的提醒與啟發。此外，我也感謝實驗室的學長姐們志承、柏瑋、崇巽、日謙、冠甫、俞慶、馨平、建佑、智程、皓軒、福源、宇哲、穩仲在實驗上的指導與關心，你們的經驗和建議都對我的成長起到了關鍵作用。我也特別感謝吳政憲學長在博士班後期，協助並教導我計畫上的執行。

我也感謝與我同時期的同學們，包括仕鎧、建傑、珮瑜、瑋駿、茂洲、凱鈞、育霖、晏

誠，我們一起共度了無數的學習時光，相互鼓勵和支持，你們是我成長道路上不可或缺的夥伴，希望未來你們也都一帆風順。此外，我也要感謝實驗室的學弟妹們，包括奕年、笠荃、冠儒、宇瑄、宇珊、于傑、偉傑、娟瑋、昱安、之稚、照玄、瑞澤、佳撰、泓邑、雯琪、景涵、沛君、家宏、亞寰、紘銘、涵羽、淳埜、奎祐、伯瑜等，感謝你們的友情、合作和激勵，讓我的博士生活更加豐富多彩，期許你們未來一切順利，保持初心並持續向前邁進。

在清華大學修課期間，我也要感謝士賢、祐萱、敏哲、冠志、志峰、敏庭、宏瑾、豐碩、怡瑩、智展、偉軒、珮如，很慶幸能夠有你們一起參與我的學習旅程，大家的支持和鼓勵為我的研究所生活增添了無數美好回憶，也讓學習變得更加有趣且充實。

此外，特別感謝財團法人國防工業發展基金會提供的獎學金，這筆支持使我能夠專注於研究，並在學業與研究上取得優異的成績。

最後，我要特別感謝我的家人，包括父親涂永政、母親吳慧真和哥哥涂建任，你們一直是我的堅強後盾，給予我無限的愛和鼓勵，使我有信心克服所有的困難，實現我的夢想。

在這份論文的結尾，我再次由衷感謝所有支持我的人。謝謝你們，我將繼續前行，繼續努力，將所學回報給社會。

涂玉發 謹識於

國立清華大學 電子工程研究所

113 年 1 月

Contents

摘要.....	i
Abstract.....	iii
致謝.....	vi
Contents	viii
Figure Captions.....	x
Table Captions.....	xiv
Chapter 1 Introduction	1
1.1 Development of Active-Matrix Displays	1
1.2 Channel Materials of Thin-Film Transistors	1
1.3 Overview of Metal Oxide Semiconductors	3
1.4 Overview of Flexible Displays	4
Reference	8
Chapter 2 Semiconductor Parameters Extraction and Electrical Characteristic Measurement System	10
2.1 Determination of Carrier Mobility	11
2.2 Determination of Threshold Voltage	12
2.3 Determination of Subthreshold Swing	13
Chapter 3 Improvement of Output Current Characteristics and HCS Reliability in a-InGaZnO TFTs by Source-Connected Field Plate	16
3.1 Introduction.....	16
3.2 Experimental Setup	18
3.3 Results and Discussion	20
3.4 Summary	24
Reference	25
Chapter 4 Improvement of NBIS Reliability in a-InGaZnO TFTs by Capped Source Structure	35
4.1 Introduction.....	35
4.2 Experimental Setup	36
4.3 Results and Discussion	37
4.4 Summary	40
Reference	42
Chapter 5 Improvement of PBS in Moist Environment and HCS Reliability in a-InGaZnO TFTs by Optimal Location of Al ₂ O ₃ Passivation	50
5.1 Introduction.....	50
5.2 Experimental Setup	51
5.3 Results and Discussion	52
5.4 Summary	56
Reference	57

Chapter 6 Investigation of SHS-Related Instability in N-Type LTPS TFTs with Variant S/D Contact Hole Densities	65
6.1 Introduction.....	65
6.2 Experimental Setup.....	66
6.3 Results and Discussion	67
6.4 Summary	71
Reference	72
Chapter 7 Investigation of Uniaxial Mechanical Bending under DBS in P-type Flexible LTPS TFTs	81
7.1 Introduction.....	81
7.2 Experimental Setup.....	82
7.3 Results and Discussion	84
7.4 Summary	88
Reference	89
Chapter 8 Conclusion.....	99
Appendix-Publication	102



Figure Captions

Chapter 1

Figure 1-1. Variant products of display applications.	5
Figure 1-2. Schematic diagram of a structure and a pixel circuit of AM-LCD.	5
Figure 1-3. Schematic diagram of a structure and a pixel circuit of AM-OLED.....	5
Figure 1-4. Hall mobility of ZnO, Ga ₂ O ₃ , and In ₂ O ₃ metal-oxide materials.	6
Figure 1-5. Phase of ZnO, Ga ₂ O ₃ , and In ₂ O ₃ metal-oxide materials.	7

Chapter 2

Figure 2-1. Multifunctional semiconductor electrical characteristic measurement system, including Agilent B1500A semiconductor parameter analyzers.	14
Figure 2-2. Cascade Microtech M150 measurement platform.	14
Figure 2-3. Low-temperature, vacuum, and atmosphere measurement platform, including Lakeshore CPX-VF microprobe stations.....	15

Chapter 3

Figure 3-1. Simplified (a) AM-OLED and (b) corresponding pixel circuits illustrate the IR voltage drop phenomenon.	28
Figure 3-2. Three-dimensional schematic diagram and optical image of a-IGZO TFTs.....	28
Figure 3-3. (a) TEM stem mode HAADF image and (b) the elemental concentration line scan profile of energy-dispersive X-ray spectroscopy (EDS) of an a-IGZO TFT.....	29
Figure 3-4. (a) TEM image of the SCFP structure in an a-IGZO TFT. Schematic diagrams of the devices with (b) STD, (c) DCFP, and (d) SCFP.....	29
Figure 3-5. I_D - V_G transfer curves of the devices with the (a) STD, (b) DCFP, and (c) SCFP structurers.	30
Figure 3-6. I_D - V_D output current characteristics of the devices with the (a) STD, (b) DCFP, and (c) SCFP structurers.....	30
Figure 3-7. SILVACO Electric-field distribution simulations under saturation conditions of the devices with the (a) STD, (b) DCFP, and (c) SCFP structures.	31
Figure 3-8. SILVACO horizontal energy bands simulations under bias conditions of $V_G = 0$ V, $V_D = 10$ V, and $V_S = 0$ V in the STD, DCFP, and SCFP structures.	32
Figure 3-9. I_D - V_G transfer curves of the devices with the (a) STD, (b) DCFP, and (c) SCFP during HCS.	32

Figure 3-10. SILVACO total current density simulations under HCS of the devices with the (a) STD, (b) DCFP, and (c) SCFP.	33
Figure 3-11. Schematic diagrams of vertical energy bands under HCS.	34
Figure 3-12. Schematic diagrams of horizontal energy bands after HCS of the devices with the (a) STD, (b) DCFP, and (c) SCFP under linear conditions.....	34

Chapter 4

Figure 4-1. An a-IGZO TFT with a schematic cross-sectional view and a TEM image.	45
Figure 4-2. The spectrum of a UVC LED.....	45
Figure 4-3. Optical images of a-IGZO TFTs with STD, capped drain, and capped source structures.....	46
Figure 4-4. I_D - V_G transfer curves of a-IGZO TFTs for symmetric STD structure in (a) forward and (b) reverse sweeps during NBIS 1000 s.	46
Figure 4-5. I_D - V_G transfer curves of a-IGZO TFTs for asymmetric structure in (a) forward (capped drain) and (b) reverse (capped source) sweeps during NBIS 1000 s.....	46
Figure 4-6. Schematic diagram and corresponding schematic energy band of an a-IGZO TFT during NBIS.....	47
Figure 4-7. SILVACO TCAD simulations of horizontal energy bands in (a) STD, (b) capped drain, and (c) capped source structures.....	47
Figure 4-8. The optimal capped source structure show that the source region of the channel remains unaffected during NBIS.....	48
Figure 4-9. SILVACO Simulated electric-field distribution of (a) the STD and (b) the capped source structures after NBIS. (c) Schematic energy band diagrams with and without hole injection are illustrated in black and red lines, respectively.....	49

Chapter 5

Figure 5-1. Optical images of a-IGZO TFTs.	60
Figure 5-2. Schematic cross-sectional views of a-IGZO TFTs of the (a) standard, (b) Al_2O_3 -passivated, and (c) outer Al_2O_3 -passivated devices.....	60
Figure 5-3. TEM images of a-IGZO TFTs of the (a) Al_2O_3 -passivated and (b) outer Al_2O_3 -passivated devices.	61
Figure 5-4. I_D - V_G transfer curves under PBS in a moist environment in the (a) standard and (b) Al_2O_3 -passivated devices.....	61
Figure 5-5. Schematic diagram of the dissociation mechanism under PBS in a moist environment in the standard device. (b) Related vertical energy band after PBS in a moist	

environment in the standard device.....	61
Figure 5-6. I_D - V_G transfer curves under HCS in the (a) standard and (b) Al_2O_3 -passivated devices.....	62
Figure 5-7. Schematic diagrams of the (a) standard and (b) Al_2O_3 -passivated devices about the ESL and PV integrity.....	62
Figure 5-8. Schematic vertical energy band diagrams under HCS in the (a) standard and (b) Al_2O_3 -passivated devices.....	63
Figure 5-9. Schematic diagram of the outer Al_2O_3 -passivated device in a moist environment..	63
Figure 5-10. I_D - V_G transfer curves under PBS in a moist environment in the outer Al_2O_3 -passivated device.....	64
Figure 5-11. I_D - V_G transfer curves under HCS in the outer Al_2O_3 -passivated device.....	64

Chapter 6

Figure 6-1. Schematic cross-sectional view and optical images of n-type LTPS TFTs.....	75
Figure 6-2. TEM image of an n-type LTPS TFT.....	75
Figure 6-3. Schematic 3D diagrams and optical images of n-type LTPS TFTs with the (a) 1C and (b) 6C structures.....	76
Figure 6-4. (a) Log I_D - V_G and (b) linear I_D - V_G of the devices with the 1C, 3C, and 6C structures.....	76
Figure 6-5. C-V curves of the devices with the 1C, 3C, and 6C structures.....	77
Figure 6-6. Schematic diagram illustrating parasitic capacitance components, C_{edge} and $C_{overlap}$	77
Figure 6-7. I_D - V_G transfer curves of the devices with the (a) 1C and (b) 6C structures before and after SHS.....	78
Figure 6-8. I_D - V_D output current characteristics of the devices with the (a) 1C and (b) 6C structures before and after SHS.....	78
Figure 6-9. Silvaco TCAD simulation of minority carrier current density in (a) a p-type and (b) an n-type LTPS TFT under SHS.....	79
Figure 6-10. COMSOL simulation of heat distribution of the devices with the (a) 1C and (b) 6C structures under SHS conditions.....	79
Figure 6-11. Physical mechanisms of the second hump in the device with the 6C structure, and related vertical energy band diagrams (a) under and (b) after SHS.....	80
Figure 6-12. Lateral energy band diagrams of the (a) first and (b) second hump mechanisms in the 6C device.....	80

Chapter 7

Figure 7-1. (a) Practical and (b) schematic flexible LTPS TFTs.	92
Figure 7-2. Optical and schematic images of the experimental setups for devices in (a) the flat state and (b) the fixed-curve bending state during DBS.....	92
Figure 7-3. Schematic diagrams of (a) flat, (b) CW, and (c) CL conditions.....	93
Figure 7-4. Time-dependent V_{TH} shift (ΔV_{TH}) in relation to the duration of the long-term fixed-curve bending of flexible LTPS TFTs under the CW and CL bending conditions.....	93
Figure 7-5. I_D-V_G transfer curves of devices during DBS under the (a) flat, (b) CW bending, and (c) CL bending conditions.	94
Figure 7-6. GI stress distribution of COMSOL simulations under the (a) CW and (b) CL bending conditions as the top views along the line A-A', labeled in figure 7-1 (b).....	95
Figure 7-7. Stress distribution of COMSOL simulations under the (c) CW and (d) CL bending conditions as the cross-sectional views along the lines B-B' and C-C',	95
Figure 7-8. (a) hole current density, (b) impact generation rate, (c) electron current density, and (d) electric field distribution of SILVACO simulations under DBS conditions.	96
Figure 7-9. I_D-V_D output current characteristics of the device in the flat state before DBS.	97
Figure 7-10. (a) Physical model, (b) schematic horizontal, and (c) vertical energy bands diagrams of the device during DBS.....	97
Figure 7-11. (a) Time-dependent g_m , max in relation to the DBS duration. (b) Distribution of the trapped electrons of the device under the CL bending condition after DBS.	98
Figure 7-12. (a) CGS and (b) CGD curves of the device during DBS under the CL bending condition.	98

Table Captions

Chapter 1

Table 1-1. Characteristics of variant channel materials in TFTs..... 6

Table 1-2. Comparison of different characteristics between Si and InGaZnO..... 7

Chapter 2

Table 2-1. Several significant semiconductor parameters. 10

